In Situ μGISAXS: I. Experimental Setup for Submicron Study of Protein Nucleation and Growth

Eugenia Pechkova,[†‡] Ronald Gebhardt,[§] Christian Riekel,[§] and Claudio Nicolini[†‡*]
[†]Nanoworld Institute, CIRSDNNOB-University of Genoa, Genoa, Italy; [‡]Fondazione EL.B.A., Rome, Italy; and [§]European Synchrotron Radiation Facility, B.P. 220, F-38043 Grenoble Cedex, France

ABSTRACT In this study, we used microbeam grazing-incidence small-angle x-ray scattering (μGISAXS) to investigate in situ protein nucleation and crystal growth assisted by a protein nanotemplate, and introduced certain innovations to improve the method. Our aim was to understand the protein nanotemplate method in detail, as this method has been shown to be capable of accelerating and increasing crystal size and quality, as well as inducing crystallization of proteins that are not crystallizable by classical methods. The nanotemplate experimental setup was used for drops containing growing protein crystals at different stages of nucleation and growth. Two model proteins, lysozyme and thaumatin, were used under unique flow conditions to differentially probe protein crystal nucleation and growth.

INTRODUCTION

Microbeam grazing-incidence small-angle x-ray scattering (μGISAXS) is a novel method (1–3) that can be used to locally investigate thin films and surfaces, and access length scales of up to several hundred nanometers (4,5). It is therefore a potentially very interesting technique for locally studying the growth of thin protein films and layers in the confined environment of a microdrop during protein crystallization (6). The unique combination of a micrometer-sized beam (1) and reflection geometry allows us to gain, in principle, two orders of magnitude in spatial resolution compared with conventional GISAXS experiments. This approach provides a very promising tool for probing protein crystal growth and nucleation at very early stages, as induced by classical (7) and Langmuir-Blodgett (LB) nanotemplate-based (8), hanging-drop, vapor-diffusion methods. Originally, this method was applied to ex situ studies of protein crystallization (6,9,10). In these ex situ experiments, the μGISAXS was measured at various time intervals in both the total scattering and the Yoneda region (2), which represents a characteristic feature of a GISAXS pattern. The Yoneda peak occurs where the exit (α_f) angle is equal to the critical angle (α_c) of the sample (α_i, $\alpha_f = \alpha_c$), which depends on the material via the real part of the refractive index and hence on the density and roughness of the layer. The relative intensities of two coupled Yoneda peaks can therefore be interpreted in terms of a buildup of layers, islands, or holes. Some very useful information about the first steps of protein nucleation and crystallization, including different mechanisms for different methods of preparation (classical hanging-drop versus LB nanotemplate), in different proteins (cytochrome versus lysozyme), has been obtained with ex situ μGISAXS (9,10). However, ex situ experiments have several drawbacks—in particular, the discontinuity of acquisition and the fast drying of the drop, as pointed out in previous studies (6,9,10)—and the need for a new in situ approach has become apparent. In this work, we introduce new methodological developments for in situ μGISAXS, using lysozyme (11) and thaumatin (12) proteins as model systems. Our main goal is to demonstrate that scattering from a growing protein layer within a microdrop can be recorded by the proper experimental configuration in real time and continuous mode directly in the crystallization well.

MATERIALS AND METHODS

The in situ μGISAXS method utilized in the experiments presented here consists of an innovative flow-through crystallization cell (Fig. 1) and an ad hoc μGISAXS experimental layout at the ID13 microfocus beamline of the European Synchrotron Radiation Facility (Grenoble, France; Figs. 2 and 3). For every experiment done in the beamline hutch, a control experiment was carried out in parallel on the bench in the beamline laboratory.

Proteins (thaumatin from *Thaumatococcus daniellii* (24 kDa, code T7638) and lysozyme from chicken egg white (14 kDa, code L6876)) were purchased from Sigma and used without further purification. All chemicals were purchased from Sigma-Aldrich (Milano, Italy). All crystallization solutions were filtered with a 0.22 μm filter.

Classical hanging-drop crystallization method

In a typical hanging-drop crystallization experiment, a 6 μL drop containing 20 mg/mL of lysozyme in 50 mM sodium acetate (NaAc) buffer (pH 4.5) and 0.45 M sodium chloride (NaCl) was placed on a siliconized glass slide and stabilized over a reservoir containing 1 mL of 0.9 M sodium chloride in the 50 mM sodium acetate buffer. For thaumatin crystallization, 6 μL hanging drop containing 7.5 mg/mL protein in 100 mM N-(2-Acetamido) iminodiacetic acid (ADA) buffer (pH 6.5) and 0.5 M Na/K tartrate was equilibrated against a reservoir containing 1 mL of 1 M Na/K tartrate in 100 mM ADA buffer. Under these conditions (controlled crystal growth), the protein crystals became visible under a light microscope in a few days.

Nanotemplate-based crystallization method

For the nanotemplate protein crystallization, protein LB nanotemplates were prepared at the Nanoworld Institute (University of Genoa, Genoa, Italy).

Submitted August 11, 2009, and accepted for publication March 15, 2010.

*Correspondence: manuscript@ibf.unige.it

Editor: Leemor Joshua-Tor.

0006-3495/10/08/1256/6 $2.00

doi: 10.1016/j.bpj.2010.03.069

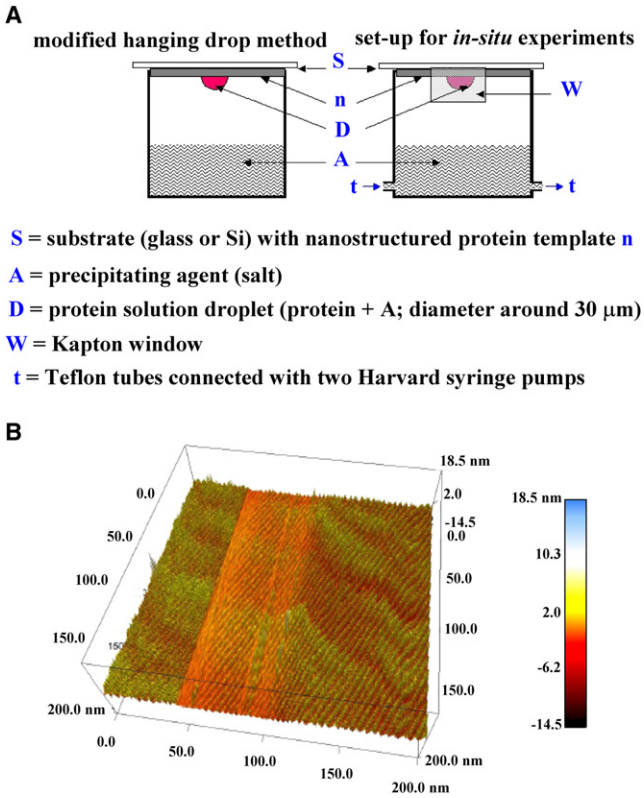

FIGURE 1 (*A*) In situ μGISAXS flow crystallization cell setup and LB nanotemplate protein crystallization method, representing a modified hanging-drop method, which employs the use of protein nanostructured LB film (n) deposited onto the glass coverslide (S) as a nanotemplate for the protein crystallization. For the flow crystallization cell, we used Kapton to construct the windows (W) for the incident and exit x-ray beam and Teflon tubes connected to Harvard syringe pumps for rapid buffer exchange. (*B*) AFM image of LB nanotemplate (2 monolayers) of thaumatin (24 kDa) at 200 nm scale.

The protein monolayer was prepared by using an in-house-built LB Teflon trough with a bath surface area of 0.44 × 0.11 m supplied with the appropriate software (13,14). A protein solution (100 mg/mL for lysozyme and 10 mg/mL for thaumatin) was prepared in distilled MilliQ water and filtered with a 0.22 μm filter. The Teflon trough was filled with pure distilled filtered MilliQ water, and a paper Wilgelmi plate was stabilized for surface pressure measurements. Protein molecules were placed at the air/water interface via a fine Hamilton 100 μL syringe (Hamilton, Reno, NV) by depositing small droplets all over the bath surface. The two-dimensional system of protein molecules at the air/water interface was compressed by two Teflon barriers with a speed of 60–70 mm/min up to a surface pressure of 25 mN/m. The dependence of the surface pressure on the barrier position (a π-A isotherm) was measured at a constant room temperature until a dense packing of molecules in the monolayer was reached. The floating monolayer was transferred onto the surface of the glass coverslide (diameter: 12 mm) by the Langmuir-Schaefer (or horizontal lift) method, in which the substrate horizontally touches the monolayer, and the layer transfers itself onto the substrate surface. The transferred layer was dried with a gaseous nitrogen flux.

The protein template thus obtained was analyzed by atomic force microscopy (AFM) (15) to estimate the regularity and uniformity of deposition. AFM is a topography-sensitive method and was used here in a noncontact tapping mode to derive topographic information from measurements of the attractive forces (Fig. 1 *B*).

The highly ordered protein nanotemplate was then utilized in the modified hanging-drop protein crystallization method (16–18). The drop was placed

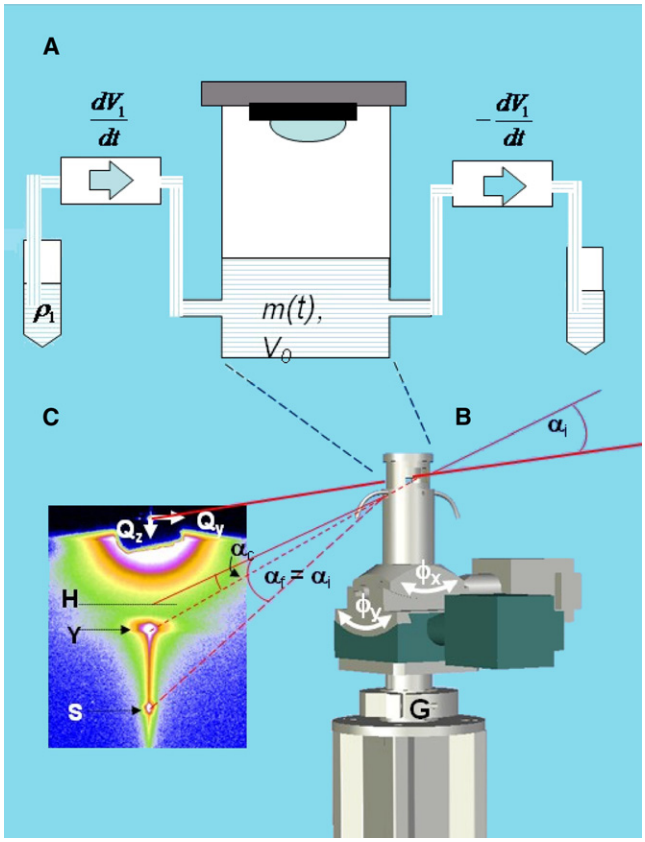

FIGURE 2 (*A*) Schematic design of the crystallization cell for studying the growth of protein crystals by the hanging-drop technique using GISAXS. (*B*) Crystallization cell installed on a goniometer stage. (*C*) Typical GISAXS pattern showing the Yoneda peak (Y) and the specular peak (S); H denotes the specimen horizon.

on the glass slide covered by the LB thin-film nanotemplate (Fig. 1 *A*). As in the classical hanging-drop method, the glass slide with the protein template and droplet was sealed with vacuum grease. The same crystallization conditions used for the classical hanging-drop method were applied.

FIGURE 3 Actual experimental setup of μGISAXS in situ, as described in the text.

A continuous experiment was conducted to monitor the in situ μGISAXS measurements with and without the LB nanotemplate. In this way, the sequence of measurements at different stages of crystallization allowed us to reconstruct the crystallization process in real time. A comparison of the results obtained by the classical and nanotemplate methods is presented in Table 1.

Flow-through crystallization cell

A modified hanging-drop crystallization cell was developed for the in situ μGISAXS experiments. The idea was to construct an ad hoc crystallization well with two windows for the incident and exit x-ray microbeam (Fig. 1 *A*) to study the protein LB nanotemplate/protein drop solution interface. The protein sample (circle glass slide covered with the LB nanotemplate, with the hanging droplet of protein solution deposited onto it) was glued onto the inner cylinder of the polystyrene crystallization well. The polystyrene inner cylinder allowed the sample to be well exposed to the windows, since it was positioned below the crystallization well border, and two kapton windows allowed scattering experiments to be performed under grazing incident conditions (Fig. 2 *A*).

The often complicated and time-consuming process of aligning the microbeam is compensated for by the ability to change the reservoir concentration, which allows one to start the crystallization process at the desired moment, accelerate the nucleation, return to the controlled-growth condition, etc. For rapid buffer exchange, the reservoir was connected via Teflon tubes with two Harvard syringe pumps (Holliston, MA). To control protein crystal nucleation and growth, these two Harvard pumps were used to quickly change the salt concentration (NaCl/buffer solution or Na/K tartrate/buffer solution) in the reservoir, which contained a volume of 0.8 mL of solution (Fig. 2). Each pump rate was set at 13 mL/h, or 3.6 μL/s.

The salt concentration in the reservoir, $m(t)$, was calculated according to the following equation:

$$m(t) = V_0 \cdot \rho_1 + (m_0 - V_0 \cdot \rho_1) \cdot e^{-\frac{\frac{dV_1}{dt}}{V_0} \cdot t}$$

The initial amount of salt in the reservoir with volume, V_0, is equal to m_0 at $t = 0$. The derivative dV_1/dt denotes the incoming volume flux with the density of salt, ρ_1. The absolute value of the outgoing flux is also dV_1/dt.

For thaumatin (used in the crystallization and buffer exchange protocol during in situ μGISAXS experiments), the following conditions were used:

In the drop: 7.5 mg/mL protein mixed with 0.5 M Na/K tartrate in 100 mM ADA buffer, pH 6.5.

In the reservoir: 0.5 M Na/K tartrate in 100 mM ADA buffer pH 6.5, stop solution, used during the alignment and the experiment preparation. To initiate the experiment with thaumatin, the reservoir solution was changed to 1 M Na/K tartrate in 100 mM ADA buffer pH 6.5.

For lysozyme, the following solutions were used:

In the drop: 20 mg/mL of protein with 0.45 M NaCl in 50 mM NaAc buffer, pH 4.5.

In the reservoir: 0.45 M NaCl in 50 mM NaAc buffer, pH 4.5 (stop solution, used during the alignment and the experiment preparation); 0.9 M NaCl in 50 mM NaAc buffer, pH 4.5 (controlled-growth solution, used in the usual crystallization protocol); and 1.8 M NaCl in 50 mM NaAc buffer, pH 4.5 (induced uncontrolled nucleation solution).

Initially, 0.45 M NaCl is kept in the drop of 6 μL against a reservoir concentration of 0.45 NaCl to establish the baseline until proper alignment of the optics and the beam is achieved. At $t = 0$ min, we bring the reservoir concentration to 1.80 M NaCl to achieve fast uncontrolled nucleation, and then at $t = 20$ min we change the reservoir salt concentration to 0.90 M NaCl to acquire a controlled crystal nucleation and growth. From $t = 24$ min until $t = 8$ h, we maintain the reservoir concentration at 0.90 M NaCl to promote the production of large crystals within a few hours (with the decrease in supersaturation rate, we promote crystal growth rather than nucleation).

μGISAXS experimental layout

The μGISAXS experiments (Fig. 3) were performed at the ID13 microfocus beamline (1) at the European Synchrotron Radiation Facility in Grenoble, France. In situ μGISAXS experiments were carried out in an experimental hutch with a very stable temperature ($\delta T = 0.2$ K; ~22°C). The monochromatic beam ($\lambda = 0.991$ Å) was focused by crossed Fresnel lenses to a spot of 0.5×1 μm^2 (full width at half-maximum) at the sample position. The size of the beam in grazing-incidence geometry is given by $S = X_v/\tan(\alpha_i)$, where α_i is the angle of incidence of the beam on the sample and X_v is the vertical beam size. For a typical angle of $\alpha_i = 0.71°$ (see below) and $X_v = 1$ μm, one calculates $S = 87$ μm. A micro-ionization chamber with a 20 μm guard aperture was used to monitor the beam intensity and reduce parasitic scattering. The flux on the sample was ~10^{10} ph/s. The direct beam was blocked by a 300 μm diameter lead beamstop. The flow-through crystallization cell was placed on a two-axis goniometer (angles: α, ψ) mounted on a motorized $x/y/z$ translation unit (Fig. 2 *B*). A fixed angle of incidence ($\alpha_i = 0.71°$) was chosen. The μGISAXS pattern was recorded by a MAR165 CCD detector (78.94 μm × 78.94 μm pixel size; 2K × 2K pixels; 16 bit readout). The sample-to-detector distance was 791 mm, as determined by a Ag-behenate standard. The μGISAXS data were acquired at time intervals of 6 min in the first 60 min, and of 10 min from 60 min up to 8 h. The shutter of the beamline was always closed, with the exception of 1 s every 6 min/h and every 10 min thereafter.

A typical μGISAXS pattern is shown in Fig. 2 *C*. Specular scattering is observed for $Q_x = Q_y = 0$, $Q_z > 0$, and diffuse scattering is seen for Q_x, $Q_y \neq 0$. Correlations vertical to the sample surface can be probed along Q_z at $Q_y = 0$. Characteristic morphological parameters, such as the shape and distances of the sample, can be extracted by analyzing out-of-plane scans in the Q_y direction, as discussed elsewhere in detail (6,9). The critical angles of lysozyme, thaumatin, and glass for the x-ray energy used were calculated on the basis of their chemical formula and densities. The Fit2D software package was used for data reduction (1). For further data analysis and generation of graphics, Sigma-Plot was used. The kinetic modeling was performed with Stella (isee systems) and Mathematica.

TABLE 1 Experimentation in the experimental hutch

THAUMATIN Time after plating	LB (number of crystals and size in microns) GS3	CLASSICAL (number of crystals and size in microns)
15 h	1 of 50, and 2 of 30	None
24 h	1 of 90 μm, 3 of 60 μm, and 20 of 20 μm	None
48 h	Several of 300 μm	Few of 100 μm
LYSOZYME	**LB (number of crystals and size in microns) GS1**	**CLASSICAL (number of crystals and size in microns) GS2**
1.5 h	1 of 10 μm	None
2.5 h	300 of 15–20 μm	None
4.5 h	300 of 30–45 μm	None
14 h	>1000 of 45–60 μm	20 crystals of ~25 μm
19.5 h	>1000 of 75 μm	2 crystals of 120 μm, and >100 crystals of 30 μm
21.5 h	>1000 of 70–80 μm, with 10 above 100 μm, filling the entire drop	150 crystals of ~90 μm, with 2 of 150 μm

RESULTS AND DISCUSSION

Initially, lysozyme was used to conduct a classical experiment at ID13 under uncontrolled-nucleation conditions

during the first 20 min, and under controlled-growth conditions for 22 h thereafter. It was consistently found that 1), the drop volume (6 μL) did not significantly change; and 2), approximately 60 crystals grew with an average crystal size of ~100 μm.

This experiment proves that under the conditions described above, we can actually perform nucleation and growth of lysozyme crystals entirely within 10 h, during which time uncontrolled lysozyme crystal-induced nucleation and controlled growth take place. Moreover, the flow-through crystallization cell permits one to avoid fast-drop evaporation as occurs in ex situ experiments.

We then conducted five different experiments in the hutch under induced-nucleation and controlled-growth conditions, as described above and summarized in Table 1:

(GS1) Lysozyme with LB film for 3 h of controlled growth.
(GS2) Lysozyme classical for 3 h of controlled growth after a very long time period for alignment.
(GS3) Thaumatin with LB film for 6 h of controlled growth.

After 48 h, parallel identical thaumatin experiments on the bench yielded threefold-larger crystals with LB compared to classical growth without LB. After 18 h, parallel experiments on the bench with lysozyme and 30 min change reservoir yielded ~100 crystals, 120 μm in length with the classical method and 300 μm with LB.

The protein templates were freshly plated in the hanging-drop container during the 1-day in situ experiment for crystal growth with the hanging-drop technique. Thin x-ray transparent windows (Fig. 3) allow entry and exit of x-ray diffraction. Hence, an optimal timing had to be found concerning the preparation, adjustment of the beam, and data acquisition time, with the footprint of the x-ray beam fully within the droplet diameter. The small (submicron) beam size avoids excessive liquid scattering and thus provides a reasonable signal/background ratio. The position of the drop relative to the beam was determined by an absorption scan with a photodiode. Experiments were performed with the beam at the center of the droplet in the droplet-protein template contact area to optimize the signal of the weakly scattering sample.

To assess the feasibility of this method, we performed preliminary experiments using either thaumatin (see Figs. 4 and 6), as discussed in depth in the companion article (12), or lysozyme (see Fig. 5). Similar results were obtained for lysozyme (11). This preliminary analysis was done only to show the feasibility of the new approach, and the reader is referred to other studies (11,12) for further details.

Fig. 4 shows an enlargement of the Yoneda region (3) of the corresponding μGISAXS pattern. This region is most sensitive to structural and morphological changes in the surface because of the interference effect involved in the occurrence of the Yoneda peak (3). The pattern is scaled to the same intensity. At the end of the kinetics, a new Yoneda peak clearly emerges next to the Yoneda peak existing at the start at a critical angle below that of the substrate.

As a working hypothesis, one can attribute the peak at higher Q_z-values to the protein itself, with the occurrence of a second Yoneda peak indicating the development of a rough layer, as previously discussed in detail for ex situ GISAXS experiments (8,9).

Detector scans were created from the two-dimensional GISAXS pattern by cutting along the Q_z axis at $Q_y = 0$. Fig. 5 shows a projection of the temporal variation of the detector cuts for lysozyme. A temporal intensity variation is observed in the angular range from 0.1° to 0.4°. Fig. 6 shows that all kinetics start with a sigmoidal increase in intensity, and that after reaching a maximum, all kinetics show a linear or exponential decrease in intensity. The first assumption from the observed detector scans is that the temporal dependence of intensities during the protein crystal growth (Fig. 6) is the sigmoidal: behavior could be due to seed formation or to the cooperative processes present in the crystal growth, and the linear or exponential decrease could be due to radiation damage. The analysis of the thaumatin Yoneda peak intensity in the experiment here reported in Fig. 6 reveals that its maximum is not exactly at the center of the Yoneda peak as it appears in the spectra reported in the

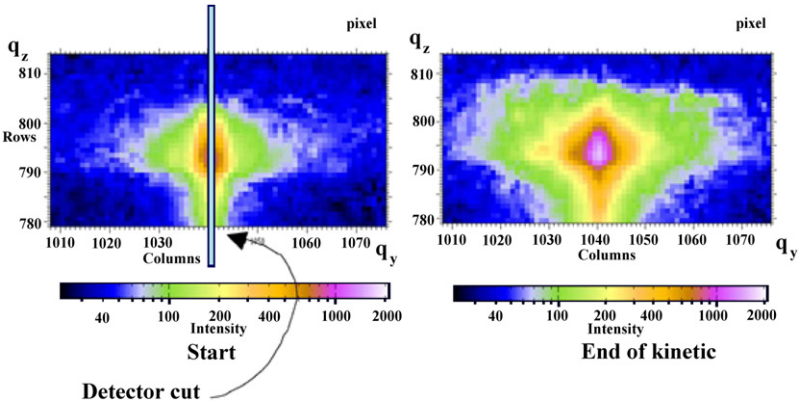

FIGURE 4 Yoneda region in the GISAXS pattern of growing thaumatin crystals in the presence of LB nanotemplate at the beginning and the end of data acquisition (discussed in detail in the accompanying article (12). Q_z increases from the top to the bottom of the graphs toward a decreasing row numbers of pixels on the detector, and Q_y, given as columns, increases to the left and right from the center of the pattern. (In captions and figures, q is in lowercase, whereas in the text and Fig. 2 *C*, uppercase Q is used.)

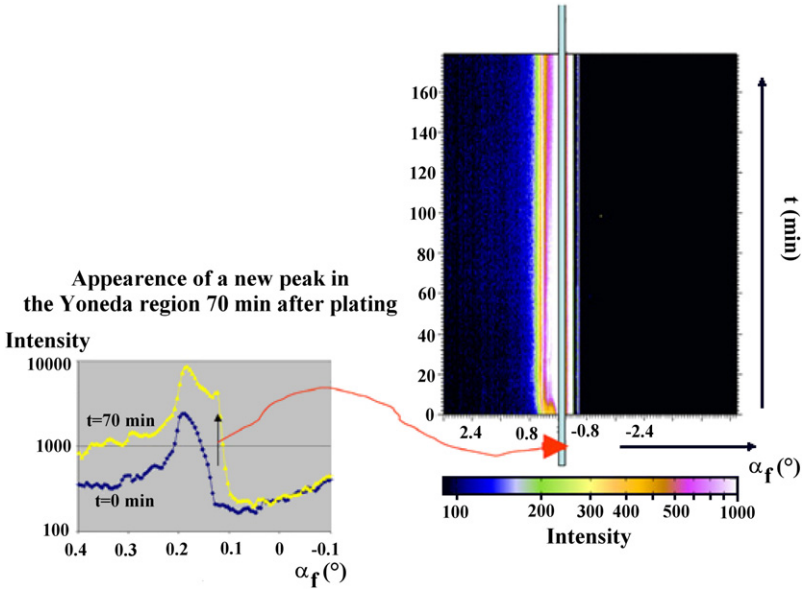

FIGURE 5 The cut on position 805 is shown to demonstrate the time evolution of the Yoneda-peak formation for lysozyme crystal. Time dependence of the detector cuts: direct beam, $\alpha_f = -0.71°$; solution scattering, $\alpha_f = -0.2°$ to $-0.5°$; Yoneda region, $\alpha_f = 0.1°$ to $0.4°$; specular beam, $\alpha_f = 0.71°$. A detector cut at fixed $q_y = 0$ reveals information about the structures vertical to the sample surface.

accompanying article (12). This is why the kinetics does not correspond exactly to the thaumatin data in Fig. 5 of Gebhardt et al. (12). Therefore, we emphasize that here we only want to demonstrate the feasibility of the approach close to the Yoneda peak of thaumatin.

The Yoneda peak consists of a contribution from glass ($\alpha_c = 0.14°$) and a contribution from protein ($\alpha_c = 0.11°$), and thus can be tentatively assumed to result from an interplay between specular and diffuse scattering. As shown in the example of lysozyme in Fig. 5, the formation of crystals can be monitored by a cut on position 805, which allows us to get the time evolution of the Yoneda peak. The observed changes could be a consequence of association/dissociation processes that take place on the LB-film surface, as shown in the accompanying article (12) and a separate study on lysozyme crystal growth (11). Their time evolution allows one to get a general idea about these processes by evaluating the temporal change of the intensity at the critical angle of the protein ($\alpha_c = 0.11°$). The kinetics of the lysozyme (Fig. 5) and thaumatin (Fig. 6) μGISAXS patterns are measured at different positions on the LB film in terms of the temporal variation of the averaged protein Yoneda peak intensity. The sigmoidal increase in intensity could be due to the seed formation, whereas the intensity decrease after reaching the maximum (Fig. 6) could be due to cooperative processes in the crystal growth resulting from radiation damage (19).

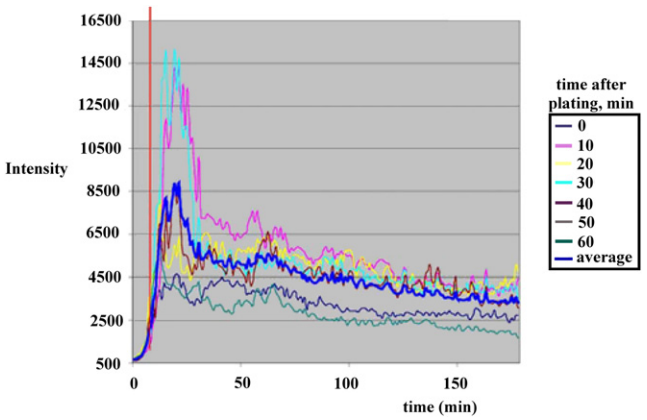

FIGURE 6 Kinetics of LB thaumatin reorganization within the crystallization microdrop. The graph shows the temporal intensity variation near the protein Yoneda peak at seven different times after plating in the Yoneda region. Of interest, all kinetics start with a sigmoidal increase in intensity, and after reaching a maximum, all kinetics show a gradual decrease in intensity.

CONCLUSIONS

In this work, we performed a feasibility study of template-assisted protein crystal growth using in situ μGISAXS, and introduced a new experimental configuration. The small droplet size used in hanging-drop experiments necessitates the use of small x-ray beams and hence the μGISAXS technique. The recording of diffuse scattering implies measuring times of up to several minutes as a result of the intensity difference of several orders of magnitude between the specularly reflected and the diffuse scattering signals. Compared to bulk protein crystallography, the enlarged beam footprint results in less radiation damage. We collected a time series of μGISAXS patterns and observed a stable μGISAXS pattern for at least up to the first few images acquired for the various experiments reported here. It appears, then, that we can exclude the possibility that the surface morphology changes are due to beam damage, based on a comparison among the different protein crystals, from either lysozyme or thaumatin. In situ development of the Yoneda peak after plating shows that the development is the result of scattering from protein-layer reorganization during crystal nucleation and growth.

Unlike topography-sensitive methods, such as AFM, μGISAXS exploits the penetration depth of x-rays. Thus, the small remaining droplet does not hinder measurement of the interface solution template, where nanocrystal growth is expected to take place. It appears that by combining grazing-incidence with wide-angle scattering to visualize crystallization (Bragg peaks), one can conduct in situ experiments with far more depth than what has been achieved by ex situ μGISAXS experiments (3–5). This in situ technique, for the first time (to our knowledge), allows one to follow protein crystal growth and nucleation from the very early stages after plating. In contrast to AFM, the hanging drop can be investigated by μGISAXS in its natural growth position without disturbing the growth process.

In summary, we have shown that, using the described innovations introduced in the flow crystallization cell and the experimental configuration of the grazing-incidence layout at the ID13 submicron x-ray beamline, we were able to record the scattering from a growing protein LB nanotemplate within a microdrop directly in situ. With this approach, the crystal nucleation and growth in hanging-drop experiments for both lysozyme (11) and thaumatin (12) can be optimally characterized, with less radiation damage.

This work was supported by an international FIRB-MIUR grant to the Nanoworld Institute (Centro Interuniversitario di Ricerca e Servizi Didattici sulle Nanotecnologie e Nanoscienze Organiche e Biologiche, University of Genoa) and an MIUR grant to the Fondazione EL.B.A. for Funzionamento.

REFERENCES

1. Riekel, C. 2000. New avenues in x-ray microbeam experiments. *Rep. Prog. Phys.* 63:233–262.
2. Muller-Buschbaum, P., S. V. Roth, …, C. Riekel. 2003. Multiple-scaled polymer surfaces investigated with micro-focus grazing-incidence small-angle X-ray scattering. *Europhys. Lett.* 61:639–645.
3. Yoneda, Y. 1963. Anomalous surface reflection of X-rays. *Phys. Rev.* 161:2010–2013.
4. Roth, S. V., M. Burghammer, …, H. Walter. 2003. Self-assembled gradient nanoparticle-polymer multilayers investigated by an advanced characterization method: microbeam grazing incidence x-ray scattering. *Appl. Phys. Lett.* 82:1935–1937.
5. Dante, S., M. DeRosa, …, V. I. Troitsky. 1996. Supramolecular ordering of bipolar lipids from Archaea in Langmuir-Blodgett films by low-angle X-ray diffraction. *Thin Solid Films.* 284:459–463.
6. Pechkova, E., S. V. Roth, …, C. Nicolini. 2005. MicroGISAXS and protein nanotemplate crystallization: methods and instrumentation. *J. Synchrotron Radiat.* 12:713–716.
7. Rosenberger, F. 1996. Protein crystallization. *J. Cryst. Growth.* 166: 40–54.
8. Nicolini, C., and E. Pechkova. 2006. Nanostructured biofilms and biocrystals. *J. Nanosci. Nanotechnol.* 6:2209–2236.
9. Nicolini, C., and E. Pechkova. 2006. Structure and growth of ultrasmall protein microcrystals by synchrotron radiation: I. microGISAXS and microdiffraction of P450scc. *J. Cell. Biochem.* 97:544–552.
10. Pechkova, E., and C. Nicolini. 2006. Structure and growth of ultrasmall protein microcrystals by synchrotron radiation: II. microGISAX and microscopy of lysozyme. *J. Cell. Biochem.* 97:553–560.
11. Pechkova, E., and C. Nicolini. 2010. In situ study of nanotemplate-induced growth of lysozyme microcrystals by submicron GISAXS. *J. Synchrotron Radiat.* submitted for publication.
12. Gebhardt, R., E. Pechkova, …, C. Nicolini. 2010. In situ GISAXS: II. Thaumatin crystal growth kinetic. *Biophys. J.*
13. Pechkova, E., and C. Nicolini. 2004. Protein nanocrystallography: a new approach to structural proteomics. *Trends Biotechnol.* 22: 599–602.
14. Pechkova, E., and C. Nicolini. 2003. Proteomics and Nanocrystallography. Kluwer Academic Press, New York.
15. Pechkova, E., M. Sartore, L. Giacomelli, and C. Nicolini. 2007. Atomic force microscopy of protein films and crystals. *Rev. Sci. Instrum.* 78:093704.
16. Pechkova, E., and C. Nicolini. 2001. Accelerated protein crystal growth by protein thin film template. *J. Cryst. Growth.* 231:599–602.
17. Pechkova, E., and C. Nicolini. 2002. Protein nucleation and crystallization by homologous protein thin film template. *J. Cell. Biochem.* 22:117–122.
18. Pechkova, E., and C. Nicolini. 2002. From art to science in protein crystallization by means of thin-film nanotechnology. *Nanotechnology.* 13:460–464.
19. Pechkova, E., S. Tripathi, …, C. Nicolini. 2009. Radiation stability of proteinase K crystals grown by LB nanotemplate method. *J. Struct. Biol.* 168:409–418.